

Dalton Transactions

Accepted Manuscript



This is an *Accepted Manuscript*, which has been through the Royal Society of Chemistry peer review process and has been accepted for publication.

Accepted Manuscripts are published online shortly after acceptance, before technical editing, formatting and proof reading. Using this free service, authors can make their results available to the community, in citable form, before we publish the edited article. We will replace this *Accepted Manuscript* with the edited and formatted *Advance Article* as soon as it is available.

You can find more information about *Accepted Manuscripts* in the [Information for Authors](#).

Please note that technical editing may introduce minor changes to the text and/or graphics, which may alter content. The journal's standard [Terms & Conditions](#) and the [Ethical guidelines](#) still apply. In no event shall the Royal Society of Chemistry be held responsible for any errors or omissions in this *Accepted Manuscript* or any consequences arising from the use of any information it contains.

A Comparison of the Amorphization of Zeolitic Imidazolate Frameworks (ZIFs) and Aluminosilicate Zeolites by Ball-milling

*Emma F. Baxter¹, Thomas D. Bennett¹, Andrew B. Cairns², Nick J. Brownbill³, Andrew L. Goodwin², David A. Keen⁴, Philip A. Chater⁵, Frédéric Blanc³ and Anthony K. Cheetham^{*1}*

¹ Department of Materials Science and Metallurgy, University of Cambridge, 27 Charles Babbage Road, Cambridge, CB3 0FS, United Kingdom

² Inorganic Chemistry Laboratory, Department of Chemistry, University of Oxford, South Parks Road, Oxford OX1 3QR, United Kingdom

³ Department of Chemistry and Stephenson Institute for Renewable Energy, University of Liverpool, Crown Street, Liverpool, L69 7ZD, United Kingdom

⁴ ISIS Facility, Rutherford Appleton Laboratory, Harwell Oxford, Didcot, OX11 0QX, United Kingdom

⁵ Diamond Light Source, Chilton, Oxfordshire OX11 0DE, United Kingdom

Abstract

X-ray diffraction has been used to investigate the kinetics of amorphization through ball-milling at 20 Hz, for five zeolitic imidazolate frameworks (ZIFs) – ZIF-8, ZIF-4, ZIF-zni, BIF-1-Li and CdIF-1. We find that the rates of amorphization for the zinc-containing ZIFs increase with increasing solvent accessible volume (SAV) in the sequence ZIF-8 > ZIF-4 > ZIF-zni. The Li-B analogue of the dense ZIF-zni amorphizes more slowly than the corresponding zinc phase, with the behaviour showing a correlation with their relative bulk moduli and SAVs. The cadmium analogue of ZIF-8 (CdIF-1) amorphizes more rapidly than the zinc counterpart, which we ascribe primarily to its relatively weak M-N bonds as well as the higher SAV. The results for

the ZIFs are compared to three classical zeolites – Na-X, Na-Y and ZSM-5 – with these taking up to four times longer to amorphize. The presence of adsorbed solvent in the pores is found to render both ZIF and zeolite frameworks more resistant to amorphization. X-ray total scattering measurements show that amorphous ZIF-zni is structurally indistinguishable from amorphous ZIF-4 with both structures retaining the same short-range order that is present in their crystalline precursors. By contrast, both X-ray total scattering measurements and ^{113}Cd NMR measurements point to changes in the local environment of amorphous CdIF-1 compared with its crystalline CdIF-1 precursor.

Keywords: Zeolitic imidazolate frameworks, zeolites, amorphization, ball-milling, mechanosynthesis.

1. Introduction

Metal-organic frameworks (MOFs) are 3D frameworks consisting of metal nodes, or clusters, bridged by organic ligands in an infinite array. The porous members of this large family are of topical interest due to their potential in a variety of applications, including carbon dioxide capture, heterogeneous catalysis and drug delivery, whilst dense MOFs are of potential interest as functional glasses and multiferroic materials.¹⁻⁴ One family of MOFs, known as the zeolitic imidazolate frameworks (ZIFs), adopt similar network topologies to zeolites, courtesy of the similar angle subtended at the bridging imidazolate ligands (Im , $\text{C}_3\text{H}_3\text{N}_2^-$) that lie between tetrahedral metal centres, when compared with the Si-O-Si angles in zeolites. The greater distance between the inorganic nodes in ZIFs ($\sim 6 \text{ \AA}$), compared to zeolites ($\sim 3 \text{ \AA}$), gives rise to larger pore diameters and higher porosities.¹

In addition to investigations into their porosity, ZIFs have been the focus of extensive work in recent years on their thermal and mechanical behaviour. These materials are mechanically soft, with the Young's moduli (E) and Hardnesses (H) of ZIFs ranging from $E = 2.97$ (de-solvated ZIF-8) to 8.49 GPa (ZIF-zni) and $H = 0.49$ (ZIF-4) to 1.08 (ZIF-zni), respectively.⁵ Those

containing substituted Im ligands, e.g. ZIF-8, which adopts a sodalite topology and utilizes 2-methylimidazole (mIm – C₄H₅N₂), are able to retain crystallinity up to temperatures exceeding 500 °C,⁶ while ZIFs based on unsubstituted Im groups will collapse upon heating to *ca.* 300 °C, and form amorphous networks, which are referred to as *a*₇ZIFs.⁷ Importantly, it has been found that porous ZIFs amorphize rapidly (in ~20 minutes) and irreversibly during ball-milling at a frequency of 30 Hz (named *a*_mZIFs),⁸ and at low pressures (~0.34 GPa) under non-hydrostatic pressure conditions.⁹ This tendency of ZIFs to amorphize may be considered a drawback for several applications, e.g. in chemical filtering, sensing and catalysis,⁸ due to the concomitant loss of framework porosity and thus adsorption capacity.¹⁰ Under certain circumstances, however, this collapse can be advantageous; for example, the *in-situ* collapse of iodine-containing ZIFs can potentially be used for the capture and retention of radioactive waste.^{11, 12}

In contrast to the ZIFs, many crystalline aluminosilicate zeolites are capable of withstanding elevated temperatures of greater than 800 °C¹³ and pressures in the range of 1.5 to 2.5 GPa.¹⁴ The more rigid mechanical properties of zeolites are illustrated by the fact that their Young's moduli (*E*) are considerably higher than those of ZIFs (e.g. ZSM-5, *E* = 57.4 GPa¹⁵). Zeolites find widespread use in industrial applications; however, a variety of factors can still influence zeolite stability, including guest cation size, ionic potential, framework topology, porosity and the Si/Al ratio.¹⁶ Furthermore, ball-milling of zeolites can cause changes in particle size,¹⁷ morphology,¹⁸ and even amorphization.¹⁹

Motivated by the dearth of detailed information on the amorphization of ZIFs compared with zeolites, we present a study on the time dependence of ball-milling induced amorphization on examples of both framework families. In order to do so, we developed a milling protocol that enables us to obtain data for both ZIFs and zeolites under the same conditions. The specific ZIF systems studied were porous ZIF-4 [Zn(Im)₂], ZIF-8 [Zn(mIm)₂] and CdIF-1 [Cd(mIm)₂] (the cadmium analogue of ZIF-8), the dense phases ZIF-zni [Zn(Im)₂] and BIF-1-Li [LiB(Im)₄] (the lithium/boron analogue of ZIF-zni). The specific zeolites studied were the important classical systems: Na-X [Na₁₆(Si_{22.4}Al₁₆O₄₈)], Na-Y [Na₇(Si₁₇Al₇O₄₈)] and Na-ZSM-5

[Na_{1.92}(Al_{1.92}Si_{22.08}O₄₈)]. Furthermore solvent effects are of great interest in the MOF community for their role in framework support,²⁰ as structure-directing agents²¹ and in catalysis.²² A subset of our work therefore focuses on the role of solvent as a structural support under ball-milling, by monitoring and comparing the amorphization rates of solvated and evacuated frameworks. In the case of ZIF-zni, where amorphization was unexpected because of the relatively low lying energy of the framework,²³ we have obtained total-scattering X-ray data for the amorphized product and compared its structure with the short range order in other *a_m*ZIFs.²⁴ In the case of the CdIF-1 system, we have used both X-rays, ¹³C and ¹¹³Cd magic angle spinning (MAS) solid state nuclear magnetic resonance (NMR) to compare the structure of the amorphous phase with that of its crystalline precursor.

2. Experimental

2.1 ZIF and Zeolite Samples

ZIF-4 is a porous open cage network which crystallizes in the orthorhombic space group *Pbca*⁶ and exhibits a solvent accessible volume (SAV) of 34.4% as calculated by the Platon programme.^{5, 25} ZIF-zni is the most thermodynamically stable member of the [Zn(Im)₂] family, possessing the same chemical formula as ZIF-4 but forming a denser, non-porous framework.²⁶ The lithium-boron analogue of ZIF-zni, BIF-1-Li, also adopts the ‘zni’ topology and both frameworks crystallizes in the space group *I4₁cd*.²⁷ Another pair of isostructural ZIFs, ZIF-8 and CdIF-1, adopt the zeolite sodalite topology^{6, 28} and are the remaining ZIF frameworks studied in the present work. Bulk samples of ZIF-4,⁶ ZIF-zni,²⁹ BIF-1-Li³⁰ and CdIF-1²⁸ (modified synthesis of CdIF-1, see Fig. S29) were synthesized following established literature procedures; ZIF-8 was purchased from BASF. Where appropriate, the ZIFs were de-solvated in a vacuum oven at 200 °C for 5 hours.

The zeolites studied in the present work were: ZSM-5, a high silica framework with the MFI topology and space group *Pnma*; Na zeolite-Y and Na zeolite-X, which both adopt the faujasite structure (FAU topology) and crystallize in space group *Fd3m*.³¹ ZSM-5 has a Si:Al ratio of

11.5, Na zeolite-Y 2.43, and Na zeolite-X 1.4. The solvent accessible volume of pure silica faujasite is 51.6% (calculated using the Platon programme²⁵), while Na zeolite-Y and Na zeolite-X have lower porosities as they contain Na⁺ in the pores. ZSM-5 has a solvent accessible volume of 31%. Na zeolite-X was synthesized according to a well-established literature procedure,³¹ and Na zeolite-Y and ZSM-5 were purchased from Zeolyst.

For the solvated framework studies, the ZIF and zeolite samples were immersed for 3 days in methanol and water, respectively, then filtered and air-dried. Thermogravimetric analysis was used to determine the quantity of solvent present in the frameworks, yielding the following results: ZIF-4 (Zn[Im]₂.1.8CH₃OH), ZIF-8 (Zn[mIm]₂.3.1CH₃OH), Na zeolite-X (Na₁₆[Si_{22.4}Al₁₆O₄₈].31H₂O), Na zeolite-Y (Na₇[Si₁₇Al₇O₄₈].29H₂O) and ZSM-5 (Na_{1.92}[Al_{1.92}Si_{22.08}O₄₈].10H₂O) (see Supplementary Information, Fig. S14-S18).

2.2 Amorphization Procedure

A ball-milling protocol was chosen following a careful evaluation of the experimental parameters that would be suitable for studying both ZIFs and the zeolites under the same conditions. Accordingly, all subsequent ball-milling was carried out by placing ~0.2 g of sample in a stainless steel grinding jar along with a 9 mm stainless steel ball. The samples were then amorphized using a milling frequency of 20 Hz in a Retsch MM400 grinder mill for a set time.

2.3 Powder X-ray Diffraction Experiments and Fractional Crystallinity Calculations

The PXRD data were collected using a Cu K α Bruker-AXS D8 diffractometer in the angular range containing peaks of interest, 2 θ 5-50°. The data were analysed and the profile fitting was carried out using the program X'pert HighScore Plus.³² X'Pert HighScore Plus was also used to determine the integral breadth of the last remaining diffraction peak in the amorphization process, with the percentage crystallinity calculated in a manner consistent with previous literature.³³ The last remaining peak is the strongest diffraction peak of the sample and the integral breadth is the ratio of the area under the peak to the peak height. The integral breadth

values rather than the full width half maximum (FWHM) values were used for the profile fitting crystallinity calculations to mitigate against the high instrumental background at low angle.

2.4 Total Scattering Experiments

Total scattering X-ray data were collected on both crystalline and amorphous samples of ZIF-zni and amorphous ZIF-4 at the I15 beamline at the Diamond Light Source, using a wavelength of $\lambda = 0.1722 \text{ \AA}$ (72 keV) and the Rapid Acquisition PDF method.³⁴ Data were collected over the angular range $0.5 < Q < 22 \text{ \AA}^{-1}$. These data were corrected for background, Compton, and multiple scattering, and beam attenuation by the sample container using the GudrunX package, which was used to normalise the 1D data to $S(Q)$ [and hence $D(r)$] rather than modelling the data itself.³⁵ The normalized structure factor $F(Q)$ was converted to the PDF in the form of the $D(r)$ function as defined in ref.³⁶ In addition, Fit2D was first used to convert the 2D diffraction image into the integrated 1D pattern.³⁷

2.5 ^{13}C and ^{113}Cd Solid-State NMR Experiments

All solid-state NMR experiments were performed on a commercial 9.4 T Bruker Avance III HD solid-state NMR spectrometer equipped with a 4 mm HXY triple-resonance MAS probe (in double resonance mode) with the ^1H channel tuned to ^1H at $\nu_0(^1\text{H}) = 400.13 \text{ MHz}$ and the X channel tuned to ^{113}Cd at $\nu_0(^{113}\text{Cd}) = 88.78 \text{ MHz}$ or ^{13}C at $\nu_0(^{13}\text{C}) = 100.03 \text{ MHz}$ or ^{15}N at $\nu_0(^{15}\text{N}) = 40.55 \text{ MHz}$. All experiments were performed under magic angle spinning (MAS) at $\nu_r = 8 \text{ kHz}$ and $T = 298 \text{ K}$. All ^1H pulses and SPINAL-64³⁸ heteronuclear decoupling were performed at a radio-frequency (rf) field amplitude of 83 kHz. ^1H - ^{113}Cd cross polarisation (CP) MAS experiments were obtained with a ^{113}Cd rf field of 46 kHz, while the ^1H rf field amplitude was ramped to obtain maximum signal at a ^1H rf field of approximately 60 kHz, and a contact time of 2 ms. ^1H - ^{13}C CP MAS experiments were obtained with a ^{13}C rf field of 45 kHz, while the ^1H rf field amplitude was ramped to obtain maximum signal at a ^1H rf field of approximately 60 kHz and a contact time of 3 ms. ^1H - ^{15}N CP MAS experiments were obtained with a ^{15}N rf field of 40 kHz, while the ^1H rf field amplitude was ramped to obtain maximum signal at a ^1H rf

field of approximately 50 kHz and a contact time of 5 ms. The ^{113}Cd spectra were referenced to 4.5 M $\text{Cd}(\text{NO}_3)_2$ in H_2O at -49.41 ppm, corresponding to 0.1 M aqueous $\text{Cd}(\text{ClO}_4)_2$ at 0 ppm.³⁹ The ^{13}C spectra were referenced to the tertiary ^{13}C of adamantane at 29.45 ppm, corresponding to TMS at 0 ppm.⁴⁰ The ^{15}N spectra were referenced to glycine at 42.40 ppm, corresponding to liquid NH_3 at 0 ppm.⁴¹ All proton spectra were referenced to water at 4.8 ppm. Samples were packed in a zirconia rotor with a Kelf cap, and NMR data were obtained and analysed using TopSpin 3.2.

2.6 Pycnometric Density Measurements

Samples densities were measured using a gas pycnometer, Micromeritics AccuPyc II 1340 (1 cm^3 model). A cycle of 10 measurements was used to calculate the mean value (including a standard deviation) for each sample.

2.7 Scanning Electron Microscopy

A field-emission scanning electron microscope, Camscan MX2600 FEGSEM, was used to record electron images of selected samples, using a working distance of 20 mm and 10 keV voltage.

2.8 Fourier Transform Infrared Spectroscopy Measurements

A Bruker Tensor 27 Infrared Spectrometer was used to carry out FT-IR analysis on the crystalline and amorphous samples. Data were collected between wavelengths of 590 and 4000 cm^{-1} . For fast data collection the spectrometer was fitted with an attenuated total reflectance cell.

3. Results and Discussion

3.1 Loss of Crystallinity of ZIFs and Zeolites during Ball-Milling

In the first set of experiments, the loss of crystallinity as a function of milling time was studied for the de-solvated zinc-containing ZIF samples, which were compared with each other and with the rates for the corresponding solvated samples (Fig. 1). Upon ball-milling of the samples, the Bragg reflections gradually decreased in intensity, as expected, resulting in the eventual formation of X-ray amorphous a_m ZIF materials (Fig. S1-S13). For convenience, the SAV values and the densities of tetrahedral sites, T/V, are tabulated for all the de-solvated systems in Table 1.

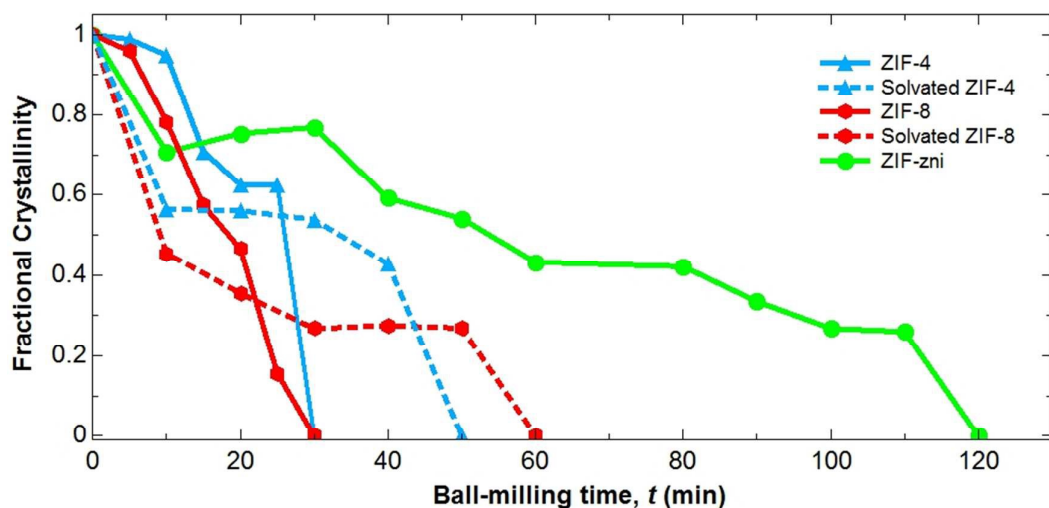


Fig. 1 Zn-containing ZIF framework crystallinity, calculated as described in the main text, plotted against time of ball-milling.

Comparison of the two de-solvated $[\text{Zn}(\text{Im})_2]$ polymorphs reveals that ZIF-4 undergoes structural collapse significantly faster than dense ZIF-zni (<30 minutes compared to ~120 minutes, Fig. 1). Indeed the latter continues to exhibit crystalline characteristics up to 110 minutes, after which a_m ZIF-zni is the sole product. The disparity in stability correlates with an increase in framework density (T/V) in ZIF-zni (4.66 nm^{-3}) compared to ZIF-4 (3.68 nm^{-3}), and a considerably smaller SAV (difference of ~22%, Table 1). ZIF-8, which has a lower T/V and higher SAV, is observed to be slightly more prone to loss of crystallinity than ZIF-4 (Fig. 1). For each of the porous ZIFs, an increase in pycnometric density was observed after milling, as seen in previous work,⁴² whereas ZIF-zni showed no significant increase in density (Table S1).

The IR spectra of the ZIF samples confirmed that the main peaks present in the crystalline ZIFs are observed in the amorphous products, which is consistent with retention of framework composition (Fig. S19-S23). As seen in previous work, a reduction in ZIF-4 particle size upon milling was detected through SEM; the crystalline particle sizes were in the range 400 to 860 nm (conglomerates of particles from 1.4 to 47 μm) and the amorphous ones 90 – 130 nm, with conglomerates from 19 – 91 μm (Fig. S27).⁴²

Our results also demonstrate how the presence of solvent in the ZIF cavities reinforces the ZIF-4 and ZIF-8 frameworks against ball-milling compared with their de-solvated counterparts (Fig. 1). The phenomenon has previously been linked to the greater elastic and bulk moduli of solvated ZIFs,⁵ a property that is linked to greater framework stability. Our findings are also consistent with a recent report on non-ZIF MOFs, where the presence of solvent in the pores prolonged the retention of crystallinity against ball-milling.⁴³ However, we also note that the solvated ZIF-4 and ZIF-8 initially loses crystallinity rather rapidly and then the rate of amorphization slows. A possible explanation for this is that during the ball-milling process we are breaking then reforming the Zn-N bonds, and this reformation step is potentially being suppressed by the presence of alternative binders, for example a solvent. Hence, whilst ball-milling of an evacuated system leads to either breaking or reformation in the original state, or breaking and reformation in a new configuration, ball-milling of a solvated one almost always excludes the first. This could potentially cause crystallinity to initially decrease faster, until a stage is reached where there are too many solvent molecules in the way of breaking further bonds.

Table 1 Physical data of de-solvated ZIF and zeolite samples along with amorphization times under ball-milling.

Sample	SAV (%)	T/V (nm ⁻³)	Reference	Time taken to amorphize the sample (minutes)
ZSM-5	-	17.97	⁴⁴	180
Na zeolite-Y	-	12.89	⁴⁵	210
Na zeolite-X	-	12.14	⁴⁵	190
ZIF-zni	7.7	4.66	¹	120
ZIF-8	50.4	2.45	¹	30
ZIF-4	34.3	3.68	¹	30
CdIF-1	55.6	2.02	²⁸	20
BIF-1-Li	5.3	5.49	²⁷	-
BIF-1-Li	5.3	5.49	²⁷	-

* - no data available. Solvent accessible volume (SAV) was calculated from the CIF files of de-solvated ZIFs using the Platon programme with a probe size radius of 1.2 Å and a grid spacing 0.2 Å.²⁵ T/V is a term commonly used to express the framework density of zeolites and now ZIFs, as the number of tetrahedral metal atoms (T) per the unit cell volume (V).⁶

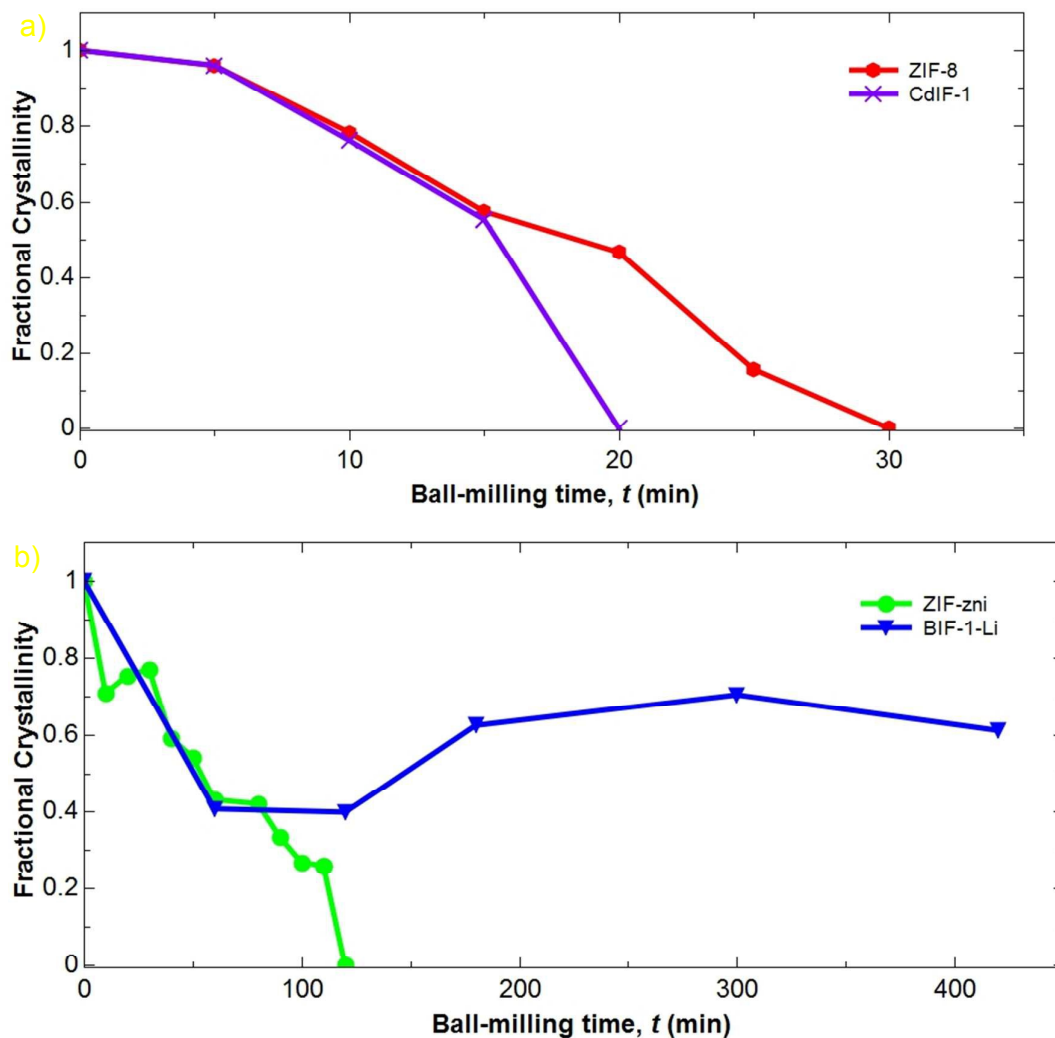


Fig. 2 Fractional crystallinities plotted against ball-milling times for a) CdIF-1 and ZIF-8, and b) ZIF-zni and BIF-1-Li.

In the next set of data (Fig. 2), we compare systems with the same topologies but different chemistries. The two sodalite frameworks, ZIF-8 and CdIF-1, amorphized rapidly under ball-milling, in 30 and 20 minutes, respectively (Fig. 2a). These results are consistent with the work of Cheetham *et al.*, where the mechanical instability of ZIF-8 is ascribed to the framework's low

shear modulus ($G_{\text{min}} \leq 1 \text{ GPa}$).⁴⁶ The greater stability of the zinc compound compared with its cadmium analogue is consistent with the known interrelationship between bond length and bond strength.⁴⁷ The shorter Zn-N bonds in ZIF-8 (1.987 Å) compared with the Cd-N bonds in CdIF-1 (2.199 Å) are expected to be stronger (bond lengths calculated using Mercury software⁴⁸), thereby accounting for the greater mechanical stability of the ZIF-8 framework against ball-milling. The T/V and SAV values also reflect how the increase in framework density and decrease in porosity result in greater resistance of the framework to ball-milling, with ZIF-8 possessing a larger T/V (2.45 nm⁻³) compared to CdIF-1 (2.02 nm⁻³), which is more porous with a larger SAV (difference of ~5%).

A second example of isostructural framework comparison is shown in Fig. 2b for ZIF-zni and BIF-Li-1. The results show BIF-Li-1 still retains some crystallinity after 7 hours of ball-milling, making it the most robust framework in the ZIF family, whereas ZIF-zni amorphizes within 120 minutes. The higher stability of BIF-Li-1 correlates with a higher framework packing density (T/V) of BIF-Li-1 (5.49 nm⁻³) compared to ZIF-zni (4.66 nm⁻³), which itself has previously been used to explain the higher bulk modulus of BIF-Li-1 under hydrostatic pressure (16 GPa) compared to ZIF-zni (14 GPa).³⁰ The fact that the Young's modulus of BIF-Li-1 is actually lower than that of ZIF-zni, suggests that the compressibility may be a more important factor in milling than uniaxial deformation.

The third set of comparisons is between the different zeolites. The main cause of instability in anhydrous zeolites has been attributed to the effects on the structure of the type and number of cations in non-framework positions,^{49, 50} though increasing the Si:Al ratio is also strongly linked to zeolite stability due to the greater strength of Si-O bonds compared to Al-O bonds.⁵¹ Our results for the two hydrated FAU zeolites, which contain identical cations and possess very similar T/V values, show that the difference in collapse times is consistent with the greater Si:Al ratio of Na zeolite-Y (2.43) compared to that of Na zeolite-X (1.4) (Fig. 3a, Table 1). However, for hydrated Na ZSM-5 the increase in Si:Al and T/V compared to the FAU systems appears to have no beneficial effect on the stability of the framework, and its behaviour is very similar to

that of Na zeolite-Y. The reason for this is not clear, though it could be related to the fact that the faujasite structure is notably incompressible for a porous structure and its bulk modulus is similar to that of much denser structures such as α -quartz.⁵²

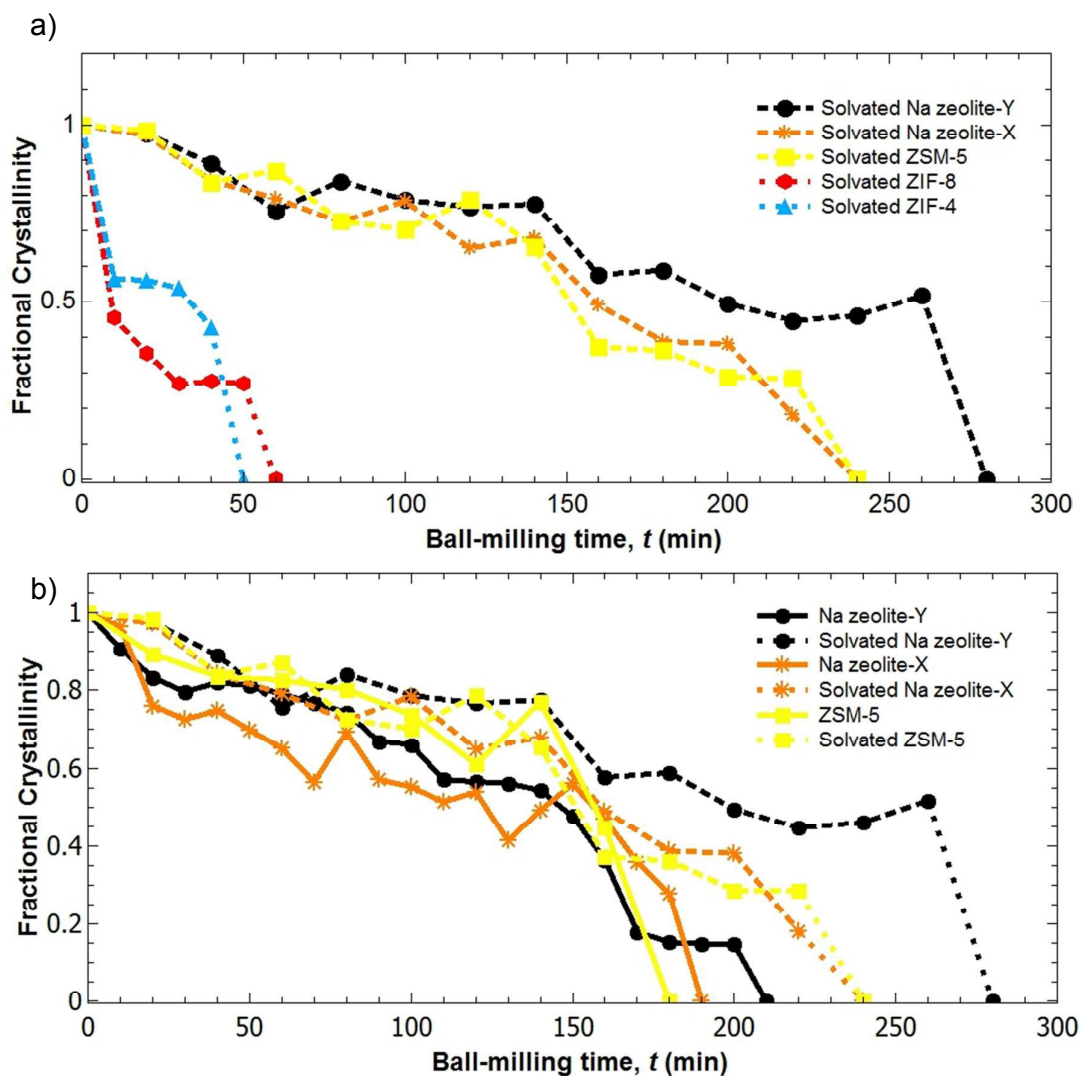


Fig. 3 a) A comparison of amorphization rates between solvated zeolites and solvated porous ZIFs under ball-milling. b) Fractional crystallinities of zeolites and solvated zeolites under ball-milling.

Removal of bulk solvent from the framework resulted in a loss of mechanical stability for all zeolites (Fig. 3b), as it did for the ZIFs. This effect was reflected in a reduction in amorphization time of 25% for Na zeolite-Y, 21% for Na zeolite-X and 25% for ZSM-5 upon

removal of bulk solvent from the zeolites. Previous work on ball-milling of ZSM-5 showed the stabilization effect of the tetrapropylammonium (TPA) cations in the ZSM-5 pores compared to activated ZSM-5.⁵³ This stabilization was attributed to the repulsive van der Waals interactions between the TPA⁺ ions and the framework. Our results show that filling of the pores by neutral water molecules is also very effective at stabilizing the zeolites.

The final comparison from the milling experiments explores the stability of ZIFs under ball-milling compared to zeolites. The results are quite striking when we compare the amorphization rates of solvated ZIFs with solvated zeolites (Fig. 3a). The least stable zeolite, Na zeolite-X (loss of crystallinity after 240 minutes) requires at least 4 times longer to amorphize compared to the most stable solvated ZIF, ZIF-8 (60 minutes). The results are consistent with the shorter and stronger bond lengths in Na zeolite-X, where the average Si/Al-O length is 1.709 Å compared to a distance of 1.987 Å in Zn-N (ZIF-8). The zeolite framework densities (T/V) of the zeolites are also 4-5 times greater than those of the porous ZIF-4 and ZIF-8 (Table 1). Our findings are also consistent with the much higher bulk moduli of zeolites, e.g. siliceous FAU is 38 GPa⁵² compared with 6.5 GPa for ZIF-8.¹¹ According to the IR data recorded for the zeolite samples, there are some differences between the crystalline spectra and those of the amorphous phases; in addition, there is evidence of hydroxide from water present in the amorphous products (Fig. S24-S26). SEM images confirm the reduction in the Na zeolite-Y particle size from 580 nm - 1000 nm to 70 – 120 nm upon ball-milling (Fig. S28), which is consistent with previous work on zeolite milling.⁵⁴

3.2 Structure of amorphous ZIF-zni (a_m ZIF-zni)

The structures of several a_m ZIFs derived from different crystalline ZIFs have been characterized previously by X-ray total scattering²⁴ and nuclear magnetic resonance,⁵⁵ but the structure of the a_m ZIF-zni has not hitherto been studied by X-ray methods. The formation of a_m ZIF-zni is interesting, given the slightly greater enthalpic stability of the crystalline framework (ZIF-zni $\Delta H_{f,298K}^\circ$ 1.31 ± 3.05 kJ mol⁻¹) compared with that of a_m ZIF-4 ($\Delta H_{f,298K}^\circ$ 5.69 ± 2.69 kJ mol⁻¹),²³

which we shall show experimentally is very similar to a_m ZIF-zni (note, however, that the amorphous phase will have a higher entropy, so the difference in free energies may be negligible at room temperature). We have therefore collected X-ray total scattering data on the ZIF-zni and the ball-milling derived a_m ZIF-zni; Fig. 4(a) compares the total scattering data of a_m ZIF-4, ZIF-zni and a_m ZIF-zni, and Fig. 4(b) shows the Pair Distribution Functions (PDFs) for the three samples.

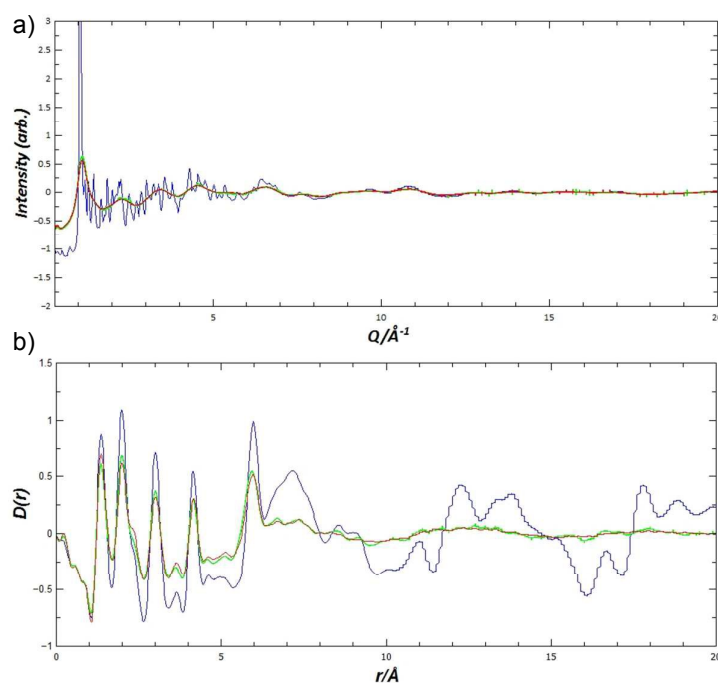


Fig. 4 Measured X-ray total scattering data for ZIF-zni (blue), a_m ZIF-zni (green) and a_m ZIF-4 (red). a) X-ray total scattering structure factors, $S(Q)$, for crystalline ZIF-zni, a_m ZIF-zni and a_m ZIF-4. b) X-ray pair distribution functions, $D(r)$, for crystalline ZIF-zni, a_m ZIF-zni and a_m ZIF-4.

Predictably, large differences in the integrated scattering patterns are observed between crystalline and amorphous samples of ZIF-zni, a_m ZIF-zni and a_m ZIF-4, with strong Bragg peaks only evident in the $S(Q)$ (Fig. 4a). However, the $S(Q)$ and PDFs of the two amorphized ZIFs are virtually indistinguishable (Fig. 4b) and the $D(r)$ traces of all three compounds have an identical

form below 6 Å (6 Å corresponds to the shortest Zn–Zn distance). This result confirms the retention of bonding within the imidazolate group and the Zn immediate coordination environment for a_m ZIF-zni, consistent with previous studies on other a_m ZIFs,²⁴ as well as recent NMR results.⁵⁵

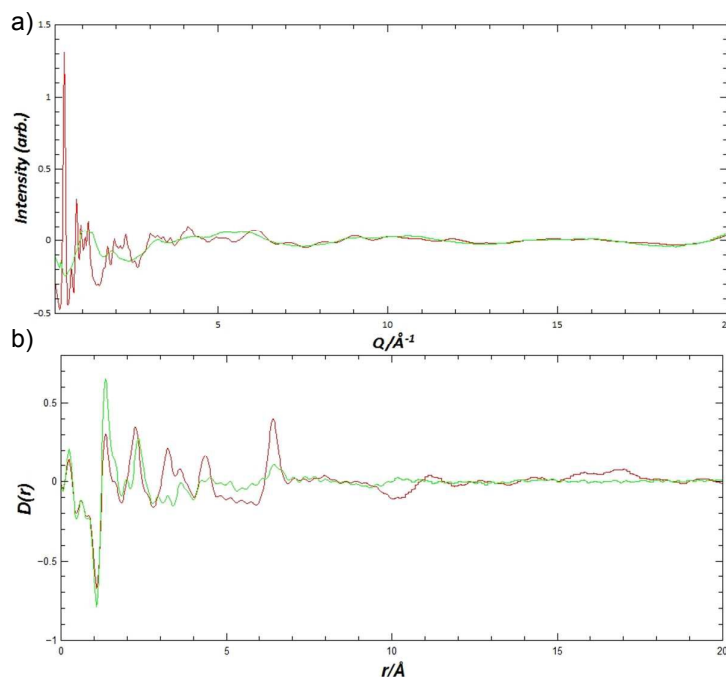


Fig. 5 Measured X-ray total scattering data for CdIF-1 (red) and a_m CdIF-1 (green) a) X-ray total scattering structure factors, $S(Q)$, for crystalline CdIF-1 and a_m CdIF-1. b) X-ray pair distribution functions, $D(r)$, for crystalline CdIF-1 and a_m CdIF-1.

3.3 Structure of amorphous CdIF-1 (a_m CdIF-1)

Similar X-ray total scattering measurements to those described in the previous section were performed on samples of CdIF-1 and a_m CdIF-1 (Fig. 5). Due to reduced data quality of a_m CdIF-1, we can only draw the following conclusions. The limit of short-range order (SRO) in CdIF-1 was found to be 6.4 Å, which is greater than the 6 Å for other Zn or Co-based amorphous ZIFs but is consistent with the M-M limit. Above this length, no real features are observed and it is clearly distinct from its crystalline parent framework (CdIF-1), which contains oscillations out to 17 Å. However, unlike the situation with the zinc-based a_m ZIFs, it is clear that the SRO up to

6.4 Å in the amorphous phase is not the same as that in the crystalline phase, suggesting that some rearrangement of the bonding around the cadmium has taken place during the milling process.

Since no evidence suggesting the decomposition or destruction of the intra-aromatic bonding upon milling exists, the ratio of the feature at 1.5 Å (belonging to intra-aromatic C-C and C-N correlations), to that of 2.2 Å (Cd-N distance), is indicative of the cadmium coordination environment in CdIF-1 and in a_m CdIF-1. Thus, the relative decrease of the intensity of the Cd-N correlation upon amorphization suggests a reduction in Cd²⁺ coordination number. By inference, the Cd²⁺ preference for 4 or 6 coordination must be restored by interactions with ligands at longer distances.

In order to shed further light on the structure of a_m CdIF-1, we performed a series of NMR studies on CdIF-1 and two samples of its amorphized derivatives, amorphized for 20 and 40 minutes (a_m CdIF-1-20 and a_m CdIF-1-40, respectively). The ¹³C CP MAS NMR spectrum of CdIF-1 is given in Fig. 6 and displays the 3 signals of the unique mIm ligands in the asymmetric unit with peaks at 13.7, 124.3 and 150.9 ppm and assigned to the CH₃, NCC and NCN carbons, respectively. All 3 NMR lines are relatively narrow (e.g. FWHM of the NCC carbon is 40 Hz) in agreement with a crystalline CdIF-1 as anticipated. The ¹³C CP MAS NMR spectra of a_m CdIF-1-20 and a_m CdIF-1-40 also show 3 resonances (15.1, 125.7 and 151.5 ppm for the CH₃, NCC and NCN carbons of mIm), but they are much broader (FWHM of the NCC carbon is 340 Hz) than in crystalline CdIF-1. This confirms that the mIm ligand is unaltered by the amorphization procedure, as observed in the NMR data of ZIF-4, ZIF-8 and ZIF-zni.⁵⁵ However, these ¹³C resonances appear at slightly different chemical shifts than in CdIF-1, supporting the existence of different local environment around the mIm in CdIF-1 and a_m CdIF-1. In addition, two resonances are observed at ~146 and ~117 ppm and correspond to the decoordination of the mIm ligands⁵⁶ from the Cd center, as observed in a_m ZIF-4.⁵⁵ Note that this process increases with ball-milling time, as evidenced by the higher intensities of the mIm ligands in a_m CdIF-1-40 than in a_m CdIF-1-20 (Fig. 6).

Close inspection of the baseline around the three ^{13}C signals in CdIF-1 (see insert in Fig. 6) reveals the presence of 3 additional broad resonances (FWHM of the NCC carbon is 300 Hz) at chemical shifts similar to those observed in a_m CdIF-1. This indicates that a portion of the crystalline CdIF-1 is amorphous, although this is not obvious from the XRD data.

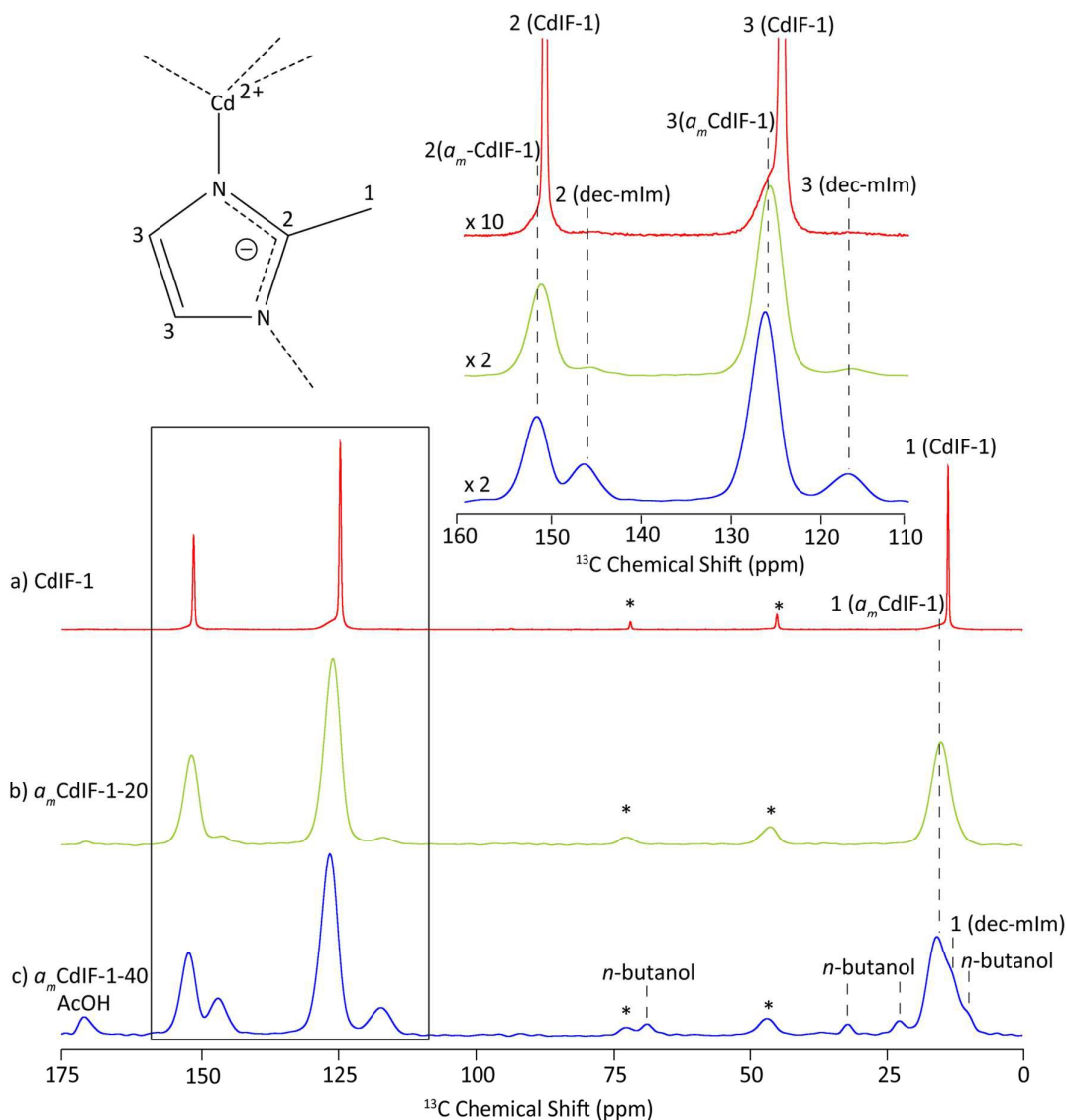


Fig. 6 ^{13}C CP MAS NMR spectra of a) CdIF-1, b) a_m CdIF-1-20 and c) a_m CdIF-1-40 obtained at 9.4 T. Spinning sidebands are marked with asterisks (*). The inset shows a magnified view (x10 in a) and x2 in b) and c)) to highlight minor features in the 160-110 ppm region. Minor residual

resonances are observed in a_m CdIF-1-40 at 11 ppm, 22 ppm, 31 ppm and 68 ppm, which are assigned to *n*-butanol, and at 171 ppm, which can be assigned to acetate moieties from the synthesis.

The ^{113}Cd CP MAS NMR spectrum of CdIF-1 is given in Fig. 7 and reveals the presence of a major sharp resonance centred at 408.3 ppm in addition to a smaller broad feature at ~ 375 ppm (see below). The presence of a single sharp resonance is consistent with the presence of only one cadmium atom in the asymmetric unit (as for its Zn counterpart ZIF-8). This line is split into a nonet with a spacing of ~ 140 Hz, which corresponds to indirect $^1\text{J}(^{113}\text{Cd}-^{14}\text{N})$ spin spin coupling between the ^{113}Cd isotope and ^{14}N (the main isotope of nitrogen, 99.63 % natural abundance with spin $I = 1$). The relative intensities of this nonet are 1:4:10:16:19:16:10:4:1 as expected for J coupling of the ^{113}Cd nucleus to four equivalent ^{14}N nuclei of the mIm ligand, confirming the 4 coordinated geometry of cadmium. The nonet given in Fig. 7 shows no shift, broadening or fine structure of each individual lines, therefore indicating that there is no evidence of second-order effects arising from residual dipolar coupling between the $I = 1/2$ ^{113}Cd nuclei and the quadrupolar ^{14}N nuclei^{57,58} (and confirmed by determination of the residual dipolar coupling constant, $d \sim 1$ Hz, which is much lower than the $^1\text{J}(^{113}\text{Cd}-^{14}\text{N}) = 140$ Hz determined here). There is an empirical relationship relating the $^1\text{J}(^{113}\text{Cd}-^{14}\text{N})$ coupling constants and the Cd-N bond distances,⁵⁷ the 140 Hz value yielding a Cd-N bond length of ~ 2.2 Å, in agreement with the 2.199 Å determined from the X-ray total scattering data (Fig. 5). The ^{15}N CP MAS NMR spectrum of CdIF-1 (Fig. S21) is dominated by a resonance at 216 ppm corresponding to the single nitrogen atom in the asymmetric unit; the doublet of 206 Hz corresponds to indirect $^1\text{J}(^{15}\text{N}-^{111,113}\text{Cd})$ spin spin coupling between ^{15}N and $^{111,113}\text{Cd}$, the two NMR active isotopes of Cd, confirming the presence of indirect $^1\text{J}(\text{N},\text{Cd})$ spin spin coupling. We note that only a doublet is observed in the ^{15}N data, rather than a doublet of doublets, due to the similar nuclear magnetic moments of the ^{111}Cd and ^{113}Cd isotopes. This is confirmed by integration of this doublet (26 % of all ^{15}N signals), which corresponds to the total natural abundance of the NMR active isotopes of Cd (12.22% and 12.80 % natural abundance of ^{111}Cd

and ^{113}Cd). The ratio of the indirect $^1J(^{113}\text{Cd}-^{14}\text{N})$ and $^1J(^{15}\text{N}-^{111,113}\text{Cd})$ coupling constants (0.68) is close to the anticipated ratio of the corresponding ^{14}N and ^{15}N nuclear magnetic moments (0.713).

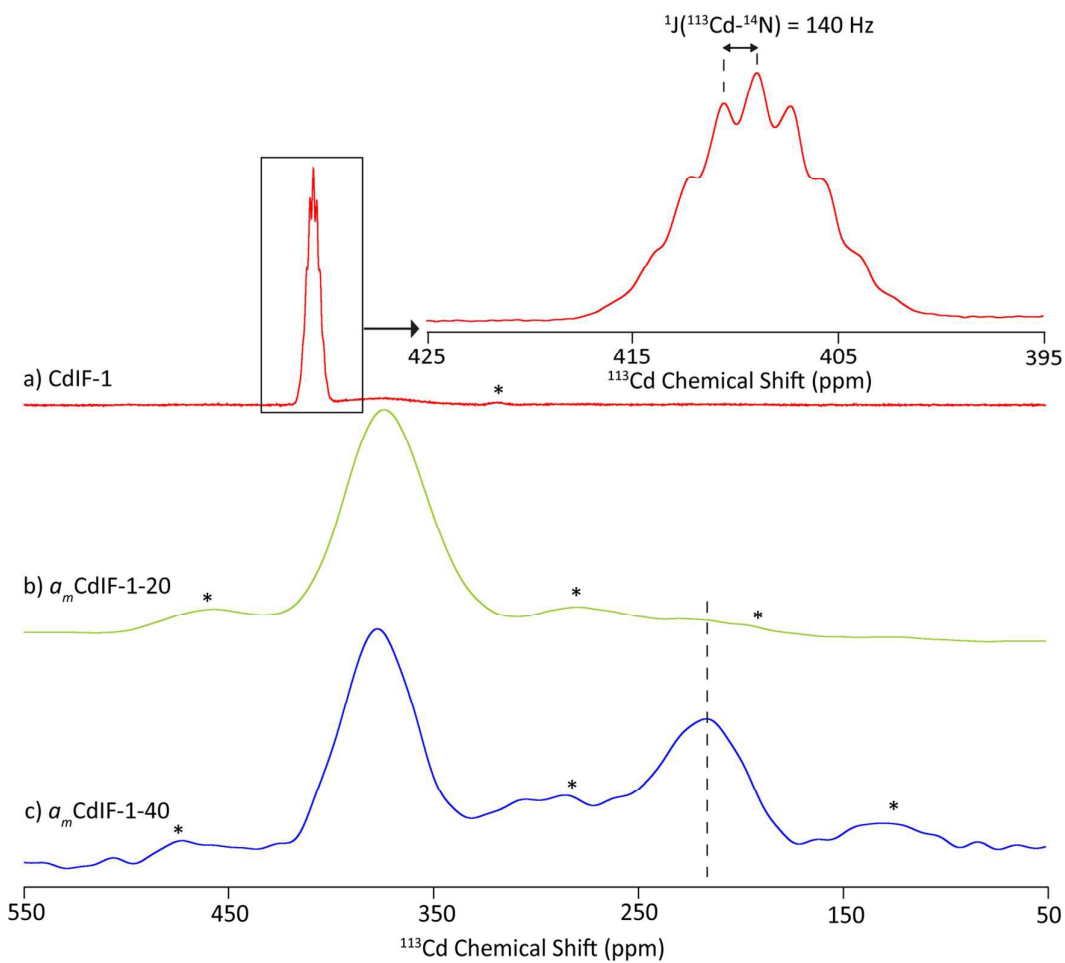


Fig. 7 ^{113}Cd CP MAS NMR spectra of a) CdIF-1 and b) a_m CdIF-1-20 and c) a_m CdIF-1-40 recorded at 9.4 T. Spinning sidebands are marked with asterisks (*). The inset shows an expanded view to highlight the multiplicity of the CdIF-1 resonance in the 425-395 ppm region reflecting the indirect $^1J(^{113}\text{Cd}-^{14}\text{N})$ spin spin coupling, and the dashed line highlights the cadmium environment at 215 ppm.

The ^{113}Cd CP MAS NMR spectrum of a_m -CdIF-1-20 (Fig. 7b) shows a broad (FWHM ~ 5300 Hz) and featureless resonance at approximately 375 ppm, corresponding to the presence of only one type of cadmium environment in the amorphous structure. The most noticeable feature is that this peak is shifted by approximately 35 ppm with respect to the ^{113}Cd signal of CdIF-1, supporting the X-ray findings that the local environment around the cadmium is different in CdIF-1 and a_m CdIF-1, unlike the situation with ZIFs. This suggests that the amorphization process is different in the two families of materials. A change of chemical shift in the NMR spectra of metals is often associated with a change of coordination number (as in ^{25}Mg , ^{27}Al , $^{69,71}\text{Ga}$),⁵⁹ but there is currently insufficient literature on ^{113}Cd NMR to yield a definitive conclusion in the present case,⁶⁰⁻⁶² in spite of a recent ^{113}Cd NMR study of cadmium-containing MOFs and some earlier work on cadmium imidazole complexes suggesting that there is a measurable relationship between ^{113}Cd chemical shift and coordination geometry.⁶³⁻⁶⁵ The broadening of the ^{113}Cd line, which probably arises from a distribution of chemical shift, prevents the detection of possible NMR line splitting due to $^1\text{J}(^{113}\text{Cd}-^{14}\text{N})$ coupling and therefore hampers the estimation of the Cd coordination number for this site.

A minor, broad resonance (FWHM ~ 5300 Hz) at approximately 215 ppm is observed in ^{113}Cd CP MAS NMR spectrum of a_m -CdIF-1-20, which could be assigned to a ^{113}Cd environment with octahedral coordination by mIm ligands; octahedral $\text{Cd}(\text{mIm})_6(\text{NO}_3)_2$ has a ^{113}Cd chemical shift of 230 ppm.⁶⁴ In the ^{113}Cd CP MAS NMR spectrum of a_m -CdIF-1-40 this peak is substantially more pronounced, at around 40% of the intensity of the main broad peak, suggesting that this species is a direct product of the ball-milling procedure.

The ^{15}N CP MAS NMR spectrum of a_m -CdIF-1-20 (Fig. S21) shows a single broad resonance with no apparent J coupling multiplicity at a chemical shift (217 ppm) at the same chemical shift than for CdIF-1.

In agreement with the ^{13}C CP MAS NMR spectrum of CdIF-1 (Fig. 6), which reveals the presence of a small amount of amorphous material, the ^{113}Cd CP MAS NMR spectrum of CdIF-

1 (Fig. 7) presents a featureless broad signal at 374 ppm that is very similar to the ^{113}Cd signal of $a_m\text{-CdIF-1}$ discussed above.

4. Conclusions

In this study we have shown, by comparing the rates of amorphization for various materials with zeolitic topologies, that ZIFs are far less resistant to structural collapse under ball-milling than their inorganic cousins in the zeolite family. For the ZIFs, the collapse time is dependent on framework density (T/V), suggesting that highly porous frameworks will not be characterized by good mechanical stability. The dense framework, ZIF-zni, still undergoes collapse to an amorphous phase, despite being the most thermodynamically stable member of the zinc-based ZIF family. Indeed, when studied by X-ray pair distribution function, the amorphous ZIF-zni phase is indistinguishable from $a_m\text{ZIF-4}$. The isostructural phases ZIF-zni and BIF-1-Li behave differently under ball-milling, with the latter being much more resistant to amorphization, which may be related to its higher bulk modulus. Replacement of zinc by cadmium in the ZIF sodalite structure also has an effect on collapse time. The SRO limit in the latter amorphous phase is greater than that in its zinc counterparts, but its lower resistance to amorphization is due to a lower T/V and weaker M-N bonds in the framework. Multinuclear ^{13}C , ^{15}N and ^{113}Cd CP MAS NMR studies indicate that the environment of cadmium is different in the CdIF-1 and its $a_m\text{CdIF-1}$ derivative, in contrast to results on zinc-containing ZIFs. Solvating the ZIFs and zeolites was shown to aid the stabilization of the frameworks against ball-milling, an effect which has been previously been shown to be effective in other MOFs.

Acknowledgements

We would like to acknowledge financial support from the Engineering and Physical Sciences Research Council, EPSRC (EFB and FB), Trinity Hall, Cambridge (TDB), the University of Liverpool (FB) the European Research Council (AKC and AK/AC), and a DTA studentship to NJB and DAK. We thank Diamond Light Source for access to beamline I15 (proposal ee9691-

1) that contributed to the PDF results presented here. We would like to thank Simon Griggs in the Department of Materials Science and Metallurgy at the University of Cambridge for help with the SEM work.

References

1. A. Phan, C. J. Doonan, F. J. Uribe-Romo, C. B. Knobler, M. O'Keeffe and O. M. Yaghi, *Acc. Chem. Res.*, 2010, **43**, 58-67.
2. U. P. N. Tran, K. K. A. Le and N. T. S. Phan, *ACS Catal.*, 2011, **1**, 120-127.
3. P. Horcajada, R. Gref, T. Baati, P. K. Allan, G. Maurin, P. Couvreur, G. Ferey, R. E. Morris and C. Serre, *Chemical reviews*, 2011, **112**, 1232-1268.
4. G. Rogez, N. Viart and M. Drillon, *Angewandte Chemie International Edition*, 2010, **49**, 1921-1923.
5. J. C. Tan, T. D. Bennett and A. K. Cheetham, *Proc. Natl. Acad. Sci. U.S.A.*, 2010, **107**, 9938-9943.
6. K. S. Park, Z. Ni, A. P. Côté, J. Y. Choi, R. Huang, F. J. Uribe-Romo, H. K. Chae, M. O'Keeffe and O. M. Yaghi, *Proc. Natl. Acad. Sci. U.S.A.*, 2006, **103**, 10186-10191.
7. T. D. Bennett, S. Cao, J. C. Tan, D. A. Keen, E. G. Bithell, P. J. Beldon, T. Friščić and A. K. Cheetham, *Journal of the American Chemical Society*, 2011, **133**, 14546-14549.
8. S. Cao, T. D. Bennett, D. A. Keen, A. L. Goodwin and A. K. Cheetham, *Chemical Communications*, 2012, **48**, 7805-7807.
9. K. W. Chapman, G. J. Halder and P. J. Chupas, *Journal of the American Chemical Society*, 2009, **131**, 17546-17547.
10. E. Proietti, F. Jaouen, M. Lefèvre, N. Larouche, J. Tian, J. Herranz and J.-P. Dodelet, *Nat. Commun.*, 2011, **2**, 416.
11. K. W. Chapman, D. F. Sava, G. J. Halder, P. J. Chupas and T. M. Nenoff, *Journal of the American Chemical Society*, 2011, **133**, 18583-18585.
12. T. D. Bennett, P. J. Saines, D. A. Keen, J.-C. Tan and A. K. Cheetham, *Chemistry- A European Journal*, 2013, **19**, 7049-7055.
13. N. Musyoka, L. Petrik, E. Hums, A. Kuhnt and W. Schwieger, *Res Chem Intermed*, 2015, **41**, 575-582.
14. Y. Huang and E. A. Havenga, *Chem. Phys. Lett.*, 2001, **345**, 65-71.
15. M. C. Johnson, J. Wang, Z. Li, C. M. Lew and Y. Yan, *Mater. Sci. Eng. A*, 2007, **456**, 58-63.
16. A. Alberti, G. Cruciani, E. Galli, R. Millini and S. Zanardi, *The Journal of Physical Chemistry C*, 2007, **111**, 4503-4511.
17. H. G. Karge and J. Weitkamp, *Zeolites as Catalysts, Sorbents and Detergent Builders: Applications and Innovations*, Elsevier Science, Amsterdam, 1989.
18. E. I. Basaldella, A. Kikot and E. Pereira, *Reactivity of Solids*, 1990, **8**, 169-177.
19. C. Kosanović, J. Bronić, B. Subotić, I. Smit, M. Stubičar, A. Tonejc and T. Yamamoto, *Zeolites*, 1993, **13**, 261-268.
20. S. Kitagawa, R. Kitaura and S.-i. Noro, *Angewandte Chemie International Edition*, 2004, **43**, 2334-2375.
21. Y.-Q. Tian, Y.-M. Zhao, Z.-X. Chen, G.-N. Zhang, L.-H. Weng and D.-Y. Zhao, *Chemistry- A European Journal*, 2007, **13**, 4146-4154.
22. C.-P. Li and M. Du, *Chemical Communications*, 2011, **47**, 5958-5972.
23. J. T. Hughes, T. D. Bennett, A. K. Cheetham and A. Navrotsky, *J. Am. Chem. Soc.*, 2013, **135**, 598-601.
24. T. D. Bennett and A. K. Cheetham, *Acc. Chem. Res.*, 2014, **47**, 1555-1562.
25. A. L. Spek, *PLATON, A Multipurpose Crystallographic Tool*, Utrecht University, the Netherlands, 1998.

26. D. W. Lewis, A. R. Ruiz-Salvador, A. Gomez, L. M. Rodriguez-Albelo, F.-X. Coudert, B. Slater, A. K. Cheetham and C. Mellot-Draznieks, *CrystEngComm*, 2009, **11**, 2272-2276.
27. J. Zhang, T. Wu, C. Zhou, S. Chen, P. Feng and X. Bu, *Angew. Chem. Int. Ed.*, 2009, **48**, 2542-2545.
28. Y.-Q. Tian, S.-Y. Yao, D. Gu, K.-H. Cui, D.-W. Guo, G. Zhang, Z.-X. Chen and D.-Y. Zhao, *Chemistry- A European Journal*, 2010, **16**, 1137-1141.
29. P. J. Beldon, L. Fábíán, R. S. Stein, A. Thirumurugan, A. K. Cheetham and T. Friščić, *Angew. Chem. Int. Ed.*, 2010, **49**, 9640-9643.
30. T. D. Bennett, J.-C. Tan, S. A. Moggach, R. Galvelis, C. Mellot-Draznieks, B. A. Reisner, A. Thirumurugan, D. R. Allan and A. K. Cheetham, *Chemistry- A European Journal*, 2010, **16**, 10684-10690.
31. J. F. Charnell, *J. Cryst. Growth*, 1971, **8**, 291-294.
32. T. Degen, M. Sadki, E. Bron, U. König and G. Nénert, *Powder Diffraction*, 2014, **29**, S13-S18.
33. V. Guillermin, F. Ragon, M. Dan-Hardi, T. Devic, M. Vishnuvarthan, B. Campo, A. Vimont, G. Clet, Q. Yang, G. Maurin, G. Férey, A. Vittadini, S. Gross and C. Serre, *Angewandte Chemie International Edition*, 2012, **51**, 9188-9188.
34. P. J. Chupas, X. Qiu, J. C. Hanson, P. L. Lee, C. P. Grey and S. J. L. Billinge, *Journal of Applied Crystallography*, 2003, **36**, 1342-1347.
35. Soper, *Technical Report RAL*, 2011, DOI: citeulike-article-id:13475858, 4915.
36. D. Keen, *J. Appl. Crystallogr.*, 2001, **34**, 172-177.
37. A. P. Hammersley, *FIT2D: An Introduction and Overview*, ESRF Internal Report, 1997.
38. B. M. Fung, A. K. Khitrin and K. Ermolaev, *J. Magn. Reson.*, 2000, **142**, 97-101.
39. G. E. Maciel and M. Borzo, *J. Chem. Soc., Chem. Commun.*, 1973, DOI: 10.1039/C3973000394A, 394a-394a.
40. C. R. Morcombe and K. W. Zilm, *J. Magn. Reson.*, 2003, **162**, 479-486.
41. R. E. Taylor and C. Dybowski, *Journal of Molecular Structure*, 2008, **889**, 376-382.
42. T. D. Bennett, S. Cao, J. C. Tan, D. A. Keen, E. G. Bithell, P. J. Beldon, T. Friscic and A. K. Cheetham, *Journal of the American Chemical Society*, 2011, **133**, 14546-14549.
43. T. D. Bennett, J. Sotelo, J.-C. Tan and S. A. Moggach, *CrystEngComm*, 2015, **17**, 286-289.
44. H. van Koningsveld, J. C. Jansen and H. van Bekkum, *Zeolites*, 1990, **10**, 235-242.
45. D. W. Breck, *Zeolite molecular sieves: structure, chemistry, and use*, R.E. Krieger, 1984.
46. J.-C. Tan, B. Civalleri, C.-C. Lin, L. Valenzano, R. Galvelis, P.-F. Chen, T. D. Bennett, C. Mellot-Draznieks, C. M. Zicovich-Wilson and A. K. Cheetham, *Physical Review Letters*, 2012, **108**, 095502.
47. J. Hornback, *Organic Chemistry*, Cengage Learning, 2005.
48. C. F. Macrae, I. J. Bruno, J. A. Chisholm, P. R. Edgington, P. McCabe, E. Pidcock, L. Rodriguez-Monge, R. Taylor, J. van de Streek and P. A. Wood, *J. Appl. Crystallogr.*, 2008, **41**, 466-470.
49. E. Dooryhee, C. R. A. Catlow, J. W. Couves, P. J. Maddox, J. M. Thomas, G. N. Greaves, A. T. Steel and R. P. Townsend, *The Journal of Physical Chemistry*, 1991, **95**, 4514-4521.
50. K. D. Hammonds, H. Deng, V. Heine and M. T. Dove, *Physical Review Letters*, 1997, **78**, 3701-3704.
51. P. A. Jacobs, E. M. Flanigen, J. C. Jansen and H. van Bekkum, *Introduction to Zeolite Science and Practice*, Elsevier Science, 2001.
52. M. Colligan, P. M. Forster, A. K. Cheetham, Y. Lee, T. Vogt and J. A. Hriljac, *Journal of the American Chemical Society*, 2004, **126**, 12015-12022.
53. C. Kosanović, A. Čižmek, B. Subotić, I. Šmit, M. Stubičar and A. Tonejc, *Zeolites*, 1995, **15**, 51-57.
54. C. Kosanović, J. Bronić, A. Čižmek, B. Subotić, I. Šmit, M. Stubičar and A. Tonejc, *Zeolites*, 1995, **15**, 247-252.

55. E. F. Baxter, T. D. Bennett, C. Mellot-Draznieks, C. Gervais, F. Blanc and A. K. Cheetham, *To be published*.
56. C. López, R. Claramunt, M. Á. García and J. Elguero, *cent.eur.j.chem.*, 2004, **2**, 660-671.
57. K. Eichele and R. E. Wasylshen, *Inorganic Chemistry*, 1994, **33**, 2766-2773.
58. S. J. Blunden, P. A. Cusack and D. G. Gillies, *Journal of Magnetic Resonance (1969)*, 1984, **60**, 114-117.
59. K. J. D. MacKenzie and M. E. Smith, *MultinuclearSolid-State NMR of Inorganic Materials* Elsevier: Oxford, Oxford, 2002.
60. M. Munataka, S. Kitagawa and F. Yagi, *Inorganic Chemistry*, 1986, **25**, 964-970.
61. I. Armitage, T. Drakenberg and B. Reilly, *Use of ¹¹³Cd NMR to Probe the Native Metal Binding Sites in Metalloproteins: An Overview*, Springer Netherlands, 2013.
62. D. L. Reger, S. S. Mason, A. L. Rheingold and R. L. Ostrander, *Inorganic Chemistry*, 1993, **32**, 5216-5222.
63. A. V. Kuttatheyil, M. Handke, J. Bergmann, D. Lässig, J. Lincke, J. Haase, M. Bertmer and H. Krautscheid, *Chemistry – A European Journal*, 2015, **21**, 1118-1124.
64. P. F. Rodesiler, N. G. Charles, E. A. H. Griffith, K. Lewinski and E. L. Amma, *Acta Crystallographica Section C*, 1986, **42**, 396-399.
65. M. F. Summers, *Coordination Chemistry Reviews*, 1988, **86**, 43-134.

Amorphization of Zeolitic Imidazolate Frameworks during ball-milling is much more rapid than that of aluminosilicate zeolites

